Control of Surface Plasmon-Polaritons in Magnetoelectric Heterostructures

Daria O. Ignatyeva, Andrey N. Kalish, Venu Gopal Achanta, Yujun Song, Vladimir I. Belotelov, and Anatoly K. Zvezdin

***Abstract*—The paper is devoted to the investigation of the surface plasmon polaritons in metal–dielectric heterostructures containing materials with magnetoelectric properties. The analysis of various possible configurations shows that the magnetoelectric effect influences the plasmonic surface wave polarization, localization, and dispersion. The essential case of Cr_2O_3 as a magnetoelectric dielectric is described in detail, revealing the switching between different regimes of magnetoelectric impact on plasmon-polaritons. Plasmonic heterostructures with magnetoelectric constituents can be used as a polarization- and dispersion-sensitive instrument to reveal the magnetoelectric coupling. Apart from that, the spin-flop effect provides an efficient tool for control of the far-field optical response of plasmonic structures by the external magnetic field.**

***Index Terms*—Antiferromagnetics, magnetoelectric effect, plasmonics.**

I. Introduction

NOWADAYS, control of surface plasmon polaritons (SPPs) by an external stimulus is of prime importance for telecommunication and other applications and is usually referred to as active plasmonics [1]–[4]. Active plasmonics utilizes strong dependence of the SPP properties, namely its dispersion, localization, the transverse profile and polarization on the permittivity of the surrounding media. Slight variations of the dielectric permittivity result in a significant shift of the SPP resonance which is widely used nowadays for sensing applications [5]–[8] and all-optical light control [9]–[14]. The impact of magneto-optical gyrotropy on the SPP properties is promising for ultrafast modulation of laser radiation [15]–[18], while the presense of optical activity [19] performs modification of the SPP polarization. It was shown that such issues of magnetoelectric coupling as chirality [20] and the axion effect in topological insulators [21] can be revealed in plasmonic structures via observation of the changes in the SPP excitation conditions or polarization mediated by them.

Modification of the SPP properties in the presense of the magnetoelectric (ME) effect is very promising in the context of the SPP control. Although surface electromagnetic waves at the interfaces of bianisotropic dielectrics have been studied earlier [22], [23], the properties of the SPP waves supported by metal/ME dielectric structures were not addressed before. At the same time, compared to the surface electromagnetic waves in dielectrics, SPPs are characterized by stronger electromagnetic field concentration in a region of about 100 nm and higher sensitivity to the medium properties which makes them promising for efficient ME light control.

In Section II of this paper we provide a theory of SPP waves in a most general case of a metal/ME dielectric interface. We provide the description and classification of different ME configurations and phases corresponding to different orientations and different types of ME crystals which makes it possible to predict the variations of SPP characteristics in the particular structure only by the form of its ME tensor. In Section III we apply our theory to Cr_2O_3 crystal which not only has the ME response but also provides the possibility to switch it due to the spin-flop effect. We analytically and numerically investigate the SPP modes in several basic configurations. We show how laser radiation can be modulated in the far-field using SPPs in ME plasmonic structures. Although the effects found in Cr_2O_3 are rather moderate, similar approach can be applied to other crystals exhibiting stronger ME response. For example, artificial metamaterials and composite multilayered structures like $BaTiO_3/CoFe_2O_4$ or $BaTiO_3/BiFeO_3$ are designed to provide the enhancement of the ME effects [24]–[27]. The structure that is characterized by the typical value of the ME constant of 0.1 has recently been designed [28], that makes the optical ME effects of practical interest.

Manuscript received November 30, 2017; revised February 27, 2018 and March 21, 2018; accepted March 24, 2018. Date of publication March 29, 2018; date of current version May 11, 2018. This work was supported in part by the Russian Foundation for Basic Research under Projects 16-02-01065 and 16-52-45061, in part by the Russian Presidential under Grant MK-2047.2017.2, and in part by the National Natural Science Foundation of China under Grant 51371018. *(Corresponding author: Andrey N. Kalish.)*

D. O. Ignatyeva, A. N. Kalish, and V. I. Belotelov are with the Faculty of Physics, Lomonosov Moscow State University, Moscow 119991 Russia, and also with the Russian Quantum Center, Moscow 121353, Russia (e-mail: ignatyeva@physics.msu.ru; kalish@physics.msu.ru; belotelov@physics.msu.ru).

V. G. Achanta is with the Tata Institute of Fundamental Research, Mumbai 400005, India (e-mail: achanta@tifr.res.in).

Y. Song is with the Beijing Key Laboratory for Magneto-Photoelectrical Composite and Interface Science, Department of Applied Physics, Center for Modern Physics Technology, University of Science and Technology Beijing, Beijing 100083, China (e-mail: songyj@ustb.edu.cn).

A. K. Zvezdin is with the Russian Quantum Center, Moscow 121353 Russia, and also with the A. M. Prokhorov General Physics Institute RAS, Moscow 119991, Russia (e-mail: zvezdin@gmail.com).

This paper has supplementary downloadable material available at http://ieeexplore.ieee.org. The file includes additional text that provides additional explanations. The total size of the file is 0.1 MB.

Color versions of one or more of the figures in this paper are available online at http://ieeexplore.ieee.org.

Digital Object Identifier 10.1109/JLT.2018.2820805

II. Theoretical Approach to the Magnetoelectric Surface Plasmon Polaritons

A. ME Effect in Cr_2O_3 Crystal

The ME effect is a coupling between the electric and magnetic field components so that the magnetic field induces electric polarization and the electric field induces magnetization in a material. It can be observed in antiferromagnetics, multiferroics, and topological insulators [29]–[32] as well as in some artificial metamaterials [24]. The following constitutive equations describe the ME effect at optical frequencies (permeability is set to unity) [26]:

$$\mathbf{D} = \hat{\varepsilon}^0 \mathbf{E} + \hat{\alpha}\mathbf{B}, \ \ \mathbf{H} = \mathbf{B} - \hat{\alpha}^+ \mathbf{E} \tag{1}$$

where $^+$ is complex conjugation, and $\hat{\alpha}$ is the ME susceptibility tensor whose symmetry and characteristic component values depend on the material. Energy conservation law requires the ME susceptibility tensor $\hat{\alpha}$ to be the same in both of equations (1) for all of the non-absorbing materials. We restrict our consideration to the case of real components of $\hat{\alpha}$.

The case of the isotropic form of the ME susceptibility tensor is similar to the so-called axion effect [33]–[35] which may appear if a perturbation breaking time reversal symmetry is present. The non-diagonal ME tensor corresponds to the toroidal type of ME response that is related to the non-zero toroidal moment and has fundamental interest for plasmonic structures [36], [37].

One of the prominent representatives of the ME materials is chromium (III) oxide Cr_2O_3 [38]. Its symmetry leads to the following form of the ME susceptibility tensor [39]:

$$\hat{\alpha} = \begin{pmatrix} \lambda_1 L_{y'} + \lambda_3 L_{z'} & \lambda_1 L_{x'} & \lambda_2 L_{x'} \\ \lambda_1 L_{x'} & -\lambda_1 L_{y'} + \lambda_3 L_{z'} & \lambda_2 L_{y'} \\ \lambda_4 L_{x'} & \lambda_4 L_{y'} & \lambda_5 L_{z'} \end{pmatrix} \tag{2}$$

where $\mathbf{L}$ is the unitary antiferromagnetic vector and λ_js are the coefficients that for the selected material have the typical values of the order of 10^{-4} [40]. This ME susceptibility tensor is written in the local coordinate system associated with the crystal symmetry: Ox' axis is parallel to the two fold axis and Oz' axis is parallel to the three fold symmetry axis (the c-axis) [41].

An important feature of Cr_2O_3 is that its ME response can be switched between two types below the Neel temperature of $T_N = 307$ K. Such switching is possible due to the "spin-flop" effect that is a reorientation of the spins in strong magnetic field applied along the three-fold axis and exceeding the threshold value of about 7 T [42]. Below the threshold, in so-called low-field phase, the spins and the antiferromagnetic vector of Cr_2O_3 both are oriented along the c-axis. At this the ME susceptibility tensor has the diagonal form, so that the electrodynamics demonstrates the axion-like behaviour. Spin-flop results in the 90° rotation of the antiferromagnetic vector that becomes perpendicular to the c-axis [40], [43]. The ME tensor in this case has non-diagonal components that affect the electrodynamics of the crystal in a different way compared to the low-field phase.

Therefore, the spin-flop is a transition from axion-like to the toroidal magnetoelectricity. Due to that, Cr_2O_3 is a unique object on which one can trace the similarities and differences between the axion-like and toroidal effects. That makes Cr_2O_3 an appropriate model object for the study of fundamental properties of ME SPPs. Due to the switchable ME effect, Cr_2O_3 is perspective for active plasmonics. Moreover, although the changes in the ME susceptibility tensor produced by spin-flop transition are rather small, it might be possible to reveal both the ME effect and the spin-flop phase transition by the sensitive SPP resonance. Therefore, the plasmonic surface of a Cr_2O_3 crystal coated with a metal, e.g., gold, provides an optical tool for investigation of the Cr_2O_3 phase transitions and allows for a light control via applied external static magnetic field.

B. General Method of the ME SPPs Analysis

For the analysis of ME SPP properties we find the eigenmodes of Maxwell's equations with the corresponding boundary conditions and constitutive equations (1) [44]. In the absence of the surface charge and the surface current the boundary conditions take the conventional forms with normal components of $\mathbf{D}$ and $\mathbf{B}$, as well as the tangential components of $\mathbf{E}$ and $\mathbf{H}$ being continuous over the interface.

The ME susceptibility tensor occuring in constitutive equations (1) can be decomposed to symmetric and antisymmetric parts: $\hat{\alpha} = \hat{\alpha}^S + \hat{\alpha}^{AS}$. Antisymmetric part is associated with the toroidal moment [39], [45] and can be expressed as:

$$\alpha_{ij}^{AS} = \epsilon_{ikj}\tau_k, \tag{3}$$

where ϵ_{ijk} is Levi-Civita symbol, and characteristic vector $\boldsymbol{\tau}$ is proportional to the toroidal moment vector $\mathbf{T}$ that is dual to $\hat{\alpha}^{AS}$.

For the most general description, the electromagnetic field of the SPP eigenmode inside of a ME dielectric is represented as the sum of the two partial TE and TM components with different polarization ($\mathbf{E}_j$) and localization (γ_j), in general, but equal propagation constants β:

$$\mathbf{E}_{\mathrm{spp}}(z>0) = \left(\mathbf{E}_{\mathrm{TM}} e^{-\gamma_{\mathrm{TM}} k_0 z} + \mathbf{E}_{\mathrm{TE}} e^{-\gamma_{\mathrm{TE}} k_0 z}\right) e^{i\beta k_0 x} \tag{4}$$

while in the metal field has the conventional form

$$\mathbf{E}_{\mathrm{spp}}(z<0) = \mathbf{E}_m e^{\gamma_m k_0 z} e^{i\beta k_0 x} \tag{5}$$

The localization coefficients and the propagation constant are normalized by vacuum wavenumber k_0. Detailed information on the ME-induced γ_j variation can be found in Supplementary. The coordinate system is chosen as shown in Fig. 1(a). For the convenience, we denote interface plane as Ξ, and SPP propagation direction as $\boldsymbol{\beta}$.

Using the above plane-wave representation for the SPP eigenmode with complex wave vector $\boldsymbol{\kappa}^{(j)} = \{\beta; 0; i\gamma_j\}$, Maxwell's equations and the consitutive equations (1) and (3) one can obtain the following wave equation:

$$[\boldsymbol{\kappa} \times [\boldsymbol{\kappa} \times \mathbf{E}]] + \hat{\varepsilon}(\boldsymbol{\kappa})\mathbf{E} = 0 \tag{6}$$

where the effective dielectric permittivity tensor $\hat{\varepsilon}(\boldsymbol{\kappa})$ that includes ME contribution has the form

$$\varepsilon_{ij}(\boldsymbol{\kappa}) = \varepsilon_{ij}^0 - (\kappa_s(\epsilon_{isk}\alpha_{kj}^S - \epsilon_{ksj}\alpha_{ik}^S) + \kappa_j\tau_i + \kappa_i\tau_j - 2(\boldsymbol{\kappa\tau})\delta_{ij}) \tag{7}$$

where δ_{ij} is Kronecker delta.

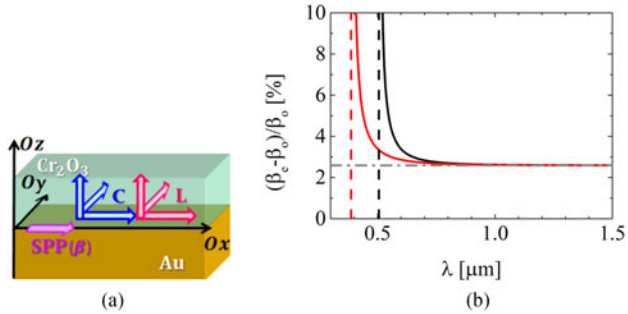

Fig. 1. (a) Possible configurations of the SPP propagation at the metal/Cr_2O_3 interface. (b) The birefringence of the SPP modes at Cr_2O_3–gold (black solid line) or silver (red solid line) interfaces. Vertical dashed lines correspond to surface plasmon frequencies ω_{sp} while gray dash-dot line shows the birefrigence asymptote. Optical parameters of metals are given in Supplementary.

The algebraic equation (6) is rather complicated, and to get clear analytical results, we apply the linear in $\hat{\alpha}$ approximation. That means, since normally $|\alpha_{ij}| << \varepsilon^0_{mn}$, we can neglect all terms that are associated with powers of α higher than first, and find the eigenmodes of (6) in the form (4), (5). Thus we obtain all the information about the ME SPP properties: polarization, localization, dispersion in the explicit form. This method is used for the analysis of the ME SPPs in all of the considered further in the paper configurations.

However in many real cases the analytical soltuion of (6) is complicated, especially in the case of the considered Cr_2O_3 that has anisotropic permittivity tensor $\hat{\varepsilon}^0$ and both symmetric and antisymmetric components of the ME susceptibility tensor. In order to reveal the impact of the symmetric and antisymmetric parts of the ME susceptibility tensor on the SPP separately, we first address the idealized problems of isotropic media with fully symmetric or fully antisymmetric ME tensors. For the simplicity, we restrict the former case to the case of isotropic ME tensor that corresponds to the so-called axion coupling.

C. Axion-Type Impact on SPPs

The impact of the axion effect on the electromagnetic wave properties reveals itself at the interface between axion and non-axion medium while the bulk electromagnetic wave does not experience the influence of the axion effect. The peculiarities of the transmission or reflection of bulk electromagnetic waves in structures with axion/non-axion layers were considered earlier [46]–[48]. We focus our attention on the SPP properties at axion-type ME/metal interface.

Here we consider an isotropic dielectric possessing the dielectric permittivity ε^0 with a diagonal ME susceptibility tensor in the form $\hat{\alpha} = \alpha\hat{I}$, where $\hat{I}$ is the identity tensor.

The analysis of the SPP properties shows that the dispersion has no linear-in-α terms so the axion effect does not noticeably change the propagation constant and the SPP resonance frequency. Since there is a polarization degeneracy of the bulk modes in a medium with the axion effect, partial TM and TE components of the SPP wave should have equal localization coefficients $\gamma_{\mathrm{TM}} = \gamma_{\mathrm{TE}}$. Notice that due to the axion coupling between the TM and TE components they are both present in the SPP field. The analytical solution of the SPP eigenmode problem (taking $H_y = 1$ here and elsewhere) gives the following expressions for the field in axion media:

$$\mathbf{E} = \begin{pmatrix} i\dfrac{\gamma_{\mathrm{TM}}}{\varepsilon^0} \\ -\alpha\dfrac{1}{\varepsilon^0 - \varepsilon_m} \\ -\dfrac{\beta}{\varepsilon^0} \end{pmatrix}, \quad \mathbf{H} = \begin{pmatrix} i\alpha\dfrac{\gamma_{\mathrm{TM}}\varepsilon_m}{\varepsilon^0(\varepsilon^0 - \varepsilon_m)} \\ 1 \\ -\alpha\beta\dfrac{\varepsilon_m}{\varepsilon^0(\varepsilon^0 - \varepsilon_m)} \end{pmatrix}. \tag{8}$$

Let us define the ratio between TE and TM components as E_y/H_y that in the case of the axion-type ME effect is $E_y/H_y = -\frac{\alpha}{\varepsilon^0 - \varepsilon_m}$. The SPP polarization ellipse in non-ME case was oriented in Oxz plane. Due to the axion-type ME effect polarization ellipse experiences the slight turn around Ox axis by an angle of $\varphi = E_y/E_z$ (since E_y and E_z are in-phase). It is important that the polarization of the SPP is constant during its propagation along the metal-dielectric interface. Similar effect was reported earlier for gyrotropic interfaces, in contrast to Faraday rotation or optical activity-caused rotation of the bulk waves. While the ME susceptibility tensor is isotropic, the direction of this polarization turn is strictly defined by the SPP propagation direction, since the angle is odd in β. This may be referred as the locking between the SPP propagation direction and the orientation of the polarization ellipse, similarly to the spin-momentum locking for electronic surface states.

Similar analysis of the SPPs at the plasmonic interface with isotropic axion-type ME effect can be directly applied to the topological insulators [21] with $\alpha = 1/137$ that possess the axion properties due to the perturbations of the time-reversal symmetry [34], [35].

D. Impact of Toroidal Magnetic Moment on SPPs

The presence of the toroidal moment leads to the effect of non-reciprocal wave propagation, so that the waves propagating along $\boldsymbol{\tau}$ and opposite to $\boldsymbol{\tau}$ possess different wavenumbers [49]. The relations between $\mathbf{E}$ and $\mathbf{H}$ vectors are also modified and, moreover, $\mathbf{E}$ and $\mathbf{H}$ vectors are generally no longer perpendicular to the wavevector. The essential point is that the impact of the toroidal moment on the bulk wave properties is polarization-independent [49], similarly to the case of the axion effect.

The properties of SPPs in media with toroidal moment are strongly dependent on the direction of $\boldsymbol{\tau}$. There are three basic configurations:

1) the longitudinal configuration: $\boldsymbol{\tau} \parallel \Xi$, $\boldsymbol{\tau} \parallel \boldsymbol{\beta}$ ($\boldsymbol{\tau} \parallel Ox$);
2) the transversal configuration: $\boldsymbol{\tau} \parallel \Xi$, $\boldsymbol{\tau} \perp \boldsymbol{\beta}$ ($\boldsymbol{\tau} \parallel Oy$);
3) the polar configuration: $\boldsymbol{\tau} \perp \Xi$ ($\boldsymbol{\tau} \parallel Oz$).

In the longitudinal configuration propagation constant and localization coefficients are affected by the toroidal moment

$$\beta = \sqrt{\frac{\varepsilon_m\varepsilon^0}{\varepsilon_m + \varepsilon^0}} - \tau_x\frac{\varepsilon_m^2}{\varepsilon_m^2 - (\varepsilon^0)^2}. \tag{9}$$

Equation (9) demonstrates the nonreciprocal propagation of the SPP: the SPPs propagating along $\boldsymbol{\tau}$ and opposite to $\boldsymbol{\tau}$ possess different propagation constants. The polarization of the SPP remains pure TM. However, the relations between the field

TABLE I
THE ME IMPACT ON THE SPP MODES IN IDEALIZED CASES

Configuration		SPP characteristics variation
The axion effect		Polarization (ellipse is tilted around Ox axis, E_y/H_y is real)
The toroidal effect	$\boldsymbol{\tau} \parallel \Xi$, $\boldsymbol{\beta} \parallel \boldsymbol{\tau}$	Dispersion (non-reciprocal), localization in both media, the eccentricity of the polarization ellipse
	$\boldsymbol{\tau} \parallel \Xi$, $\boldsymbol{\beta} \perp \boldsymbol{\tau}$	Polarization (ellipse is tilted around Oz axis, E_y/H_y is imag.)
	$\boldsymbol{\tau} \perp \Xi$	Localization depth in dielectric

components inside the dielectric are slightly modified

$$\mathbf{E} = \begin{pmatrix} i\dfrac{1}{\sqrt{-(\varepsilon_m+\varepsilon^0)}} - i\tau_x\dfrac{\sqrt{-\varepsilon_m\varepsilon^0}}{\varepsilon_m^2-(\varepsilon^0)^2} \\ 0 \\ -\sqrt{\dfrac{\varepsilon_m}{\varepsilon^0(\varepsilon_m+\varepsilon^0)}} + \tau_x\dfrac{\varepsilon^0}{\varepsilon_m^2-(\varepsilon^0)^2} \end{pmatrix}, \ \mathbf{H} = \begin{pmatrix} 0 \\ 1 \\ 0 \end{pmatrix}. \tag{10}$$

It follows from (10) that if the SPP propagates along $\boldsymbol{\tau}$ the electric field components diminish and, moreover, the polarization ellipse becomes narrower as its semiaxes ratio E_x/E_z gets smaller. At the same time, the semiaxes ratio of the polarization ellipse for the metal E_z/E_x also diminishes. For the opposite direction of the SPP propagation the results are opposite.

In the polar configuration only localization constant for the dielectric changes upon the toroidal moment. Since the configuration is isotropic in the interface plane, the SPP propagation is reciprocal and the field components remain unchanged.

On the contrary, in the transversal configuration the propagation constant and the localization coefficients are independent of the toroidal moment. At the same time, the SPP polarization acquires TE components. Due to the optical isotropy $\gamma_{\rm TM} = \gamma_{\rm TE}$. The field inside the dielectric has a form

$$\mathbf{E} = \frac{1}{\varepsilon^0}\begin{pmatrix} i\gamma_{\rm TM} \\ i\tau_y\dfrac{\beta}{\gamma_{\rm TM}+\gamma_m} \\ -\beta \end{pmatrix}, \ \mathbf{H} = \begin{pmatrix} -\tau_y\dfrac{\gamma_m\beta}{\varepsilon^0(\gamma_{\rm TM}+\gamma_m)} \\ 1 \\ i\tau_y\dfrac{\varepsilon^0-\gamma_{\rm TM}\gamma_m}{\varepsilon^0(\gamma_{\rm TM}+\gamma_m)} \end{pmatrix} \tag{11}$$

so the TE/TM ratio is $E_y/H_y = i\tau_y\sqrt{-\frac{\varepsilon_m}{\varepsilon^0}}\frac{1}{\varepsilon^0-\varepsilon_m}$.

The plane of the polarization ellipse turns around Oz axis by the angle of $\varphi = E_y/E_x$ compared to the non-toroidal case (unlike the case of the axion effect, E_x and E_y are in-phase), and upon the toroidal moment reversal the polarization ellipse turns in the other direction.

The results of Sections II-C and II-D are summarized in Table I.

III. SURFACE PLASMON POLARITONS AT THE METAL/Cr_2O_3 INTERFACE: OPTICAL ANISOTROPY AND MAGNETOELECTRICITY

A. General Features of the SPP at the Metal/Cr_2O_3 Interface

The observed impact of the ME effect in a Cr_2O_3 crystal on the SPP modes depends significantly on the relative orientation of the crystal c-axis and the antiferromagnetic vector $\mathbf{L}$ with respect to the plasmonic interface Ξ between a metal and the Cr_2O_3 crystal as well as with respect to the direction of the SPP propagation $\boldsymbol{\beta}$. For the detailed analysis we choose 9 basic possible configurations of the SPP propagation along the interface [see Fig. 1(a)] which correspond to 3 possible orientations of the c-axis and 3 possible orientations of $\mathbf{L}$ vector with respect to $\boldsymbol{\beta}$ direction.

Cr_2O_3 crystal possesses optical anisotropy, for the wavelength of 633 nm $\varepsilon_\perp = 4.9$ and $\varepsilon_\parallel = 5.15$ [41] where $\varepsilon_\perp$ and $\varepsilon_\parallel$ are components of $\hat{\varepsilon}^0$ corresponding to the perpendicular or parallel to the c-axis directions. Therefore the dispersion of the SPP waves at its interface depends on crystal orientation. In the case of c-axis $\parallel \Xi$, $\boldsymbol{\beta} \perp c$-axis, the SPP can be called "ordinary" since it does not experience anisotropy:

$$\beta_o = \sqrt{\frac{\varepsilon_\perp\varepsilon_m}{\varepsilon_\perp+\varepsilon_m}}. \tag{12}$$

In the other cases optical anisotropy affects the SPP and its "extraordinary" dispersion takes the following forms:

$$\beta_e = \sqrt{\frac{\varepsilon_m\varepsilon_\parallel(\varepsilon_m-\varepsilon_\perp)}{\varepsilon_m^2-\varepsilon_\perp\varepsilon_\parallel}} \tag{13}$$

if the c-axis is oriented perpendicular to the interface Ξ; and

$$\beta_e = \sqrt{\frac{\varepsilon_m\varepsilon_\perp(\varepsilon_m-\varepsilon_\parallel)}{\varepsilon_m^2-\varepsilon_\perp\varepsilon_\parallel}} \tag{14}$$

if $\boldsymbol{\beta} \parallel c$-axis. Such dependence of the dispersion on the orientation of the anisotropic crystal was presented in [50].

Numerical estimations of the SPP mode "birefringence" for the two perpendicular $\boldsymbol{\beta}$ directions in the case of c-axis $\parallel \Xi$ [see Fig. 1(b)] show that the difference between the wavenumbers of the two modes increases near the surface plasmon frequency $\omega_{\rm sp}$ at which $\beta(\omega_{\rm sp}) = \infty$. There is a slight difference between the surface plasmon frequencies of the two modes according to (12) and (14). For example, for the gold/Cr_2O_3 interface the surface plasmon frequency corresponds to $\lambda_{\rm sp\,e} = 506$ nm and $\lambda_{\rm sp\,o} = 503.5$ nm while for the silver/Cr_2O_3 interface $\lambda_{\rm sp\,e} = 390$ nm and $\lambda_{\rm sp\,o} = 387$ nm. For higher wavelengths ($\lambda > 900$ nm for the considered structure) the birefrigence reaches its asymptote $(\beta_e - \beta_o)/\beta_o = \sqrt{\varepsilon_\parallel/\varepsilon_\perp} - 1$ and equals $2.6\,\%$ in Cr_2O_3.

The analysis of the SPP mode characteristics in Cr_2O_3/metal structure with the corresponding ME response was performed as described in Section II-B. Table II summarizes its results showing which changes in mode properties corresponding to the certain configurations and the crystal phases are observed. The analytical expressions for the corresponding changes are rather complicated nevertheless Table II gives an overview of the nature of the ME impact on the SPP modes. Further we discuss several configurations in a more detailed way and perform numerical simulations using the following values for the ME coefficients: $\lambda_1 = 1.6 \cdot 10^{-4}$, $\lambda_2 = 1.0 \cdot 10^{-4}$, $\lambda_3 = -1.965 \cdot 10^{-4}$, $\lambda_5 = -0.82 \cdot 10^{-4}$ [41].

TABLE II
CHARACTERISTICS OF SPP MODES THAT ARE AFFECTED BY THE ME EFFECT IN Cr_2O_3/METAL STRUCTURE FOR VARIOUS CONFIGURATIONS AND PHASES

<table>
<tr><td colspan="4">$c \perp$ interface</td></tr>
<tr><td rowspan="2">The low-field phase ($\mathbf{L} \parallel c$)</td><td colspan="3">The spin-flop phase ($\mathbf{L} \perp c$)</td></tr>
<tr><td colspan="2">SPP $\perp$ $\mathbf{L}$</td><td>SPP $\parallel$ $\mathbf{L}$</td></tr>
<tr><td>polarization ($\frac{E_y}{H_y}$ is real)</td><td colspan="2">dispersion
localization</td><td>polarization ($\frac{E_y}{H_y}$ is imag.), localization in dielectric</td></tr>
<tr><td colspan="4">$c \parallel$ interface</td></tr>
<tr><td rowspan="3">The low-field phase ($\mathbf{L} \parallel c$), any SPP direction</td><td colspan="3">The spin-flop phase ($\mathbf{L} \perp c$)</td></tr>
<tr><td colspan="2">$\mathbf{L} \perp$ interface</td><td rowspan="2">$\mathbf{L} \parallel$ interface, any SPP direction</td></tr>
<tr><td>SPP $\parallel$ c</td><td>SPP $\perp$ c</td></tr>
<tr><td>polarization ($\frac{E_y}{H_y}$ is real)</td><td>polarization ($\frac{E_y}{H_y}$ is imag.) localization in dielectric</td><td>dispersion
localization</td><td>localization in dielectric</td></tr>
</table>

B. SPP Polarization in the Low-Field Phase of Cr_2O_3

Let us discuss ME SPP properties in the low-field phase of Cr_2O_3 (which means $\mathbf{L} \parallel c$-axis). This case corresponds to the axion effect described in Section II-C, therefore one should expect change only in SPP polarization. In both possible basic low-field configurations: $\mathbf{L} \parallel c$-axis $\parallel \Xi$ and $\mathbf{L} \parallel c$-axis $\perp \Xi$, the SPP mode has both nonzero TM and TE components with different localization coefficients that are independent of magnetoelectric susceptibility tensor components. The TE/TM ratio for the "extraordinary" SPP (for the case c-axis $\perp \Xi$) inside Cr_2O_3 is

$$\frac{E_y}{H_y} = \frac{\lambda_5 - \lambda_3}{\varepsilon_\perp - \varepsilon_\parallel} - \left[(\gamma_m + \gamma_{\mathrm{TM}}) \frac{\lambda_5 - \lambda_3}{\varepsilon_\perp - \varepsilon_\parallel} + \gamma_{\mathrm{TM}} \frac{\lambda_5}{\varepsilon_\perp} \right] \frac{e^{-(\gamma_{\mathrm{TE}} - \gamma_{\mathrm{TM}})|z|}}{\gamma_m + \gamma_{\mathrm{TE}}} \tag{15}$$

The analogous expression can be obtained for the "ordinary" SPP

$$\frac{E_y}{H_y} = \frac{\lambda_5 - \lambda_3}{\varepsilon_\perp - \varepsilon_\parallel} - \left[\frac{\lambda_5 - \lambda_3}{\varepsilon_\perp - \varepsilon_\parallel} + \frac{\lambda_3 \gamma_{\mathrm{TM}}}{\varepsilon_\perp (\gamma_{\mathrm{TE}} + \gamma_m)} \right] e^{-(\gamma_{\mathrm{TE}} - \gamma_{\mathrm{TM}})|z|} \tag{16}$$

The polarization ellipse turns around Ox axis (that coincides with $\boldsymbol{\beta}$) with respect to the non-ME case, see Fig. 2(a) (E_y and E_z are in-phase). At the same time according to (15), (16) the polarization of the SPP depends on z inside Cr_2O_3. According to the simulations presented in Fig. 2(c) and (d) in both cases the TE/TM ratio increases with the distance to the interface and at $k_0 z = 0.5$ is significantly higher than at the interface.

Near-field polarization of the "extraordinary" SPP in the low-field phase demonstrates very peculiar behaviour. For the spectral range from 506 nm to 711 nm polarization ellipse tilt changes its sign inside the ME crystal. At the wavelength of 712 nm the polarization of the SPP is purely TM exactly at the metal-dielectric interface and is twisting with the distance inside Cr_2O_3. Such polarization behaviour inside Cr_2O_3 described by (15), (16) is a result of the difference in localization coeffients for TM and TE components.

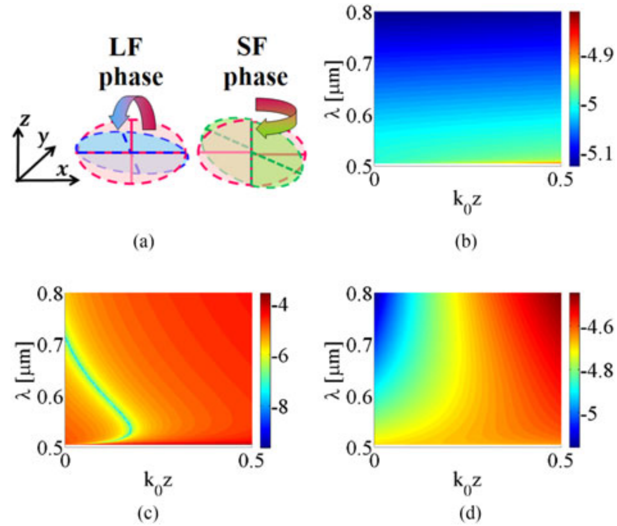

Fig. 2. (a) The schematic representation of the corresponding tilt of the polarization ellipse for the low-field (LF) and spin-flop (SF) phases; (b–d) the dependence of the cross-section polarization of the ME SPP ($\lg|E_y/H_y|$) on wavelength in the cases of: (b) the spin-flop phase, extraordinary SPP; (c) the low-field phase, extraordinary SPP; (d) the low-field phase, ordinary SPP.

C. SPP Polarization in the Spin-Flop Phase of Cr_2O_3

The polarization ellipse tilt can be observed in the spin-flop ($\mathbf{L} \perp c$-axis) phase of Cr_2O_3, for example, in the configuration $\boldsymbol{\beta} \parallel \mathbf{L}$, c-axis $\perp \Xi$. Comparison of (2) and (3) reveals that in this configuration the emerged toroidal moment $\boldsymbol{\tau} \parallel \Xi$ and $\boldsymbol{\tau} \perp \boldsymbol{\beta}$ (see Table I).

The TE/TM ratio in this configuration can be described as follows:

$$\frac{E_y}{H_y} = -i \frac{\lambda_2}{e^{-\gamma_{\mathrm{TM}}|z|}} \cdot \left[\frac{\gamma_{\mathrm{TM}}}{\varepsilon_\perp \beta} e^{-\gamma_{\mathrm{TM}}|z|} + \frac{1}{\varepsilon_\perp \beta} \frac{\varepsilon_\perp - \gamma_{\mathrm{TM}} \gamma_m}{\gamma_m + \gamma_{\mathrm{TE}}} e^{-\gamma_{\mathrm{TE}}|z|} \right] \tag{17}$$

The polarization ellipse experiences a slight turn around Oz axis with respect to the non-ME case, see Fig. 2(a) (E_y and E_x are in-phase). At the same time, the SPP polarization is inhomogeneous in its cross-section analogous to the case of the low-field phase [see Fig. 2(b)] due to the difference between γ_{TE} and γ_{TM}.

D. SPP Dispersion and Non-reciprocity in the Spin-flop Phase of Cr_2O_3

For definiteness we consider the following configuration: the c-axis $\perp \Xi$, $\boldsymbol{\beta} \uparrow\uparrow Ox$, $\mathbf{L} \uparrow\uparrow Oy$. At this, the toroidal moment $\boldsymbol{\tau} \parallel \boldsymbol{\beta}$ and according to Table I in this case one may observe the non-reciprocal propagation constant variation due to the ME

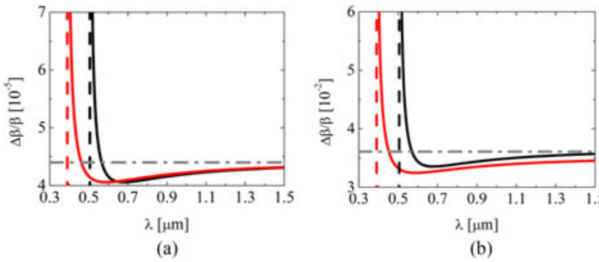

Fig. 3. The ME-induced variation of the SPP dispersion (a) for the spin-flop phase of $\mathrm{Cr_2O_3}$, and (b) for the material with $\alpha = 0.08$ (see details in the text). Red and black solid lines correspond to silver and gold interfaces, respectively. Dashed lines correspond to surface plasmon frequencies ω_{sp} and dash-dot line shows the asymptote for $\Delta\beta/\beta$.

effect. For the SPP propagating along the positive direction of Ox axis the propagation constant has the form

$$\beta = \sqrt{\frac{\varepsilon_m \varepsilon_\parallel (\varepsilon_m - \varepsilon_\perp)}{\varepsilon_m^2 - \varepsilon_\parallel \varepsilon_\perp}} - \lambda_2 \frac{\varepsilon_m^2}{\varepsilon_m^2 - \varepsilon_\parallel \varepsilon_\perp} \tag{18}$$

while opposite $\boldsymbol{\beta}$ would have the opposite sign of ME contribution to the propagation constant $\Delta\beta$ (the second term in (18)). This nonreciprocity $\Delta\beta/\beta$ for the considered configuration is presented in Fig. 3(a). Note that $\Delta\beta/\beta$ increases at the wavelengths near the surface plasmon frequency ω_{sp} and has an asymptote $\Delta\beta/\beta = \lambda_2/\sqrt{\varepsilon_\parallel}$ for higher wavelengths.

$\mathrm{Cr_2O_3}$ possesses rather low values of the ME constants that are of about 10^{-4}. Recently artificial structures have been constructed that exhibit ME properties with the characteristic value of 0.1 so all the effects described in the present paper are significantly enhanced. An example is shown in Fig. 3(b) where the giant non-reciprocity, i.e., ME-induced SPP dispersion variation, is shown for the material with $\epsilon = 5.5$ and $\alpha = 0.08$. These parameters correspond to the $\mathrm{BaTiO_3/BiFeO_3}$ superlattice fabricated in [28]. The ME nonreciprocity is about 10^{-2} that is three orders higher than for $\mathrm{Cr_2O_3}$ [see Fig. 3(a)].

E. Far-field Control Using ME SPPs

The analysis performed above shows how the ME properties of the material provide the variations of the SPP near-field properties. These variations can also be observed in the far-field as the variation of the reflectance spectra of the ME plasmonic structure. Namely, there are two straightforward ways to get the far-field response from the SPP modulation:

1) Dispersion-based measurements: This scheme can be implemented only in the spin-flop phase $\boldsymbol{\beta} \perp \mathbf{L} \perp c$ (see Table II) so that ME coupling changes the propagation constant of the SPP. The shift of the SPP resonance position is determined by the SPP dispersion variation due to application of the external magnetic field $\mathbf{H}$ which causes the spin re-orientation in ME crystal. This shift results in the variation of the angular reflectance spectra which can be measured as

$$\delta = \frac{R(\mathbf{H}) - R(0)}{R(\mathbf{H}) + R(0)}. \tag{19}$$

This idea is very similar to the well-known transverse magneto-optical Kerr effect in magnetic plasmonic structures [51].

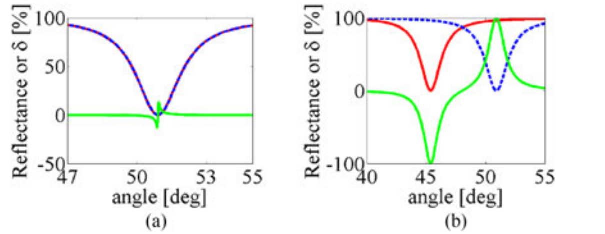

Fig. 4. Reflectance angular spectra (blue and red curves for low-field and spin-flop phase, correspondingly) and its variation δ (green curve) due to ME switching calculated (a) for $\mathrm{Cr_2O_3}$, and (b) for the material with $\alpha = 0.08$ (see details in the text).

For example, ME SPPs excited at 800 nm wavelength using Kretchmann scheme via GaP prism at the $\mathrm{Cr_2O_3}$/gold interface in low-field and spin-flop phase provide relative reflectance modulation $\delta = 13\%$, see Fig 4(a), and thus can be measured using ordinary experimental techniques. For $\mathrm{BaTiO_3/BiFeO_3}$ superlattice reported in [28] incorporated instead of $\mathrm{Cr_2O_3}$ in the same scheme, relative modulation depth is up to 100%, see Fig. 4(b). Such scheme with ME SPPs can be used not only for efficient modulation of the signal, but for the magnetic-field controlled deflection of the laser beams as well.

2) Polarization-based measurements: Since in certain cases (see Table II) a tilt of SPP polarization ellipse is observed, one can measure this tilt using either polarization or reflectance measurements. Namely, a rotation of the polarization of the reflected light can be measured (which is similar to the magneto-optical Faraday effect) or variation of the reflectance spectra due to the excitation efficiency change of the SPP with tilted polarization ellipse. Moreover, such ME SPPs can be excited using TE-polarized incident light thus providing the possibility for imaging of the spin-flop effect. However the observed polarization-based far-field effects depend on the square of the ME constant and are less pronounced than the dispersion-based measurements.

IV. Conclusion

We have performed the original thorough research of the ME influence on the SPPs. We have shown how one can predict and qualitatively analyze the variations of SPP characteristics in the particular structure only by the form of its ME tensor. We have applied this results to the important special case of the metal/$\mathrm{Cr_2O_3}$ interface.

Two revealed nonreciprocal ME effects are of prime importance for managing of the optical response of the plasmonic structures. The first one is locking between the SPP propagation direction and the polarization ellipse tilt direction due to nonreciprocity, similar to the spin-momentum locking for electronic surface states. The second one is nonreciprocal variation of the SPP propagation constant. It is promising for active control of the far-field optical response of the plasmonic structure by switching of the external magnetic field. Additionally, this phenomenon can be used to observe the phase transitions from the low-field to the spin-flop phase. Using the materias with high ME response in the plasmonic structure, one may perform the magnetic-field controlled deflection of the laser beams as well.

References

[1] K. F. MacDonald, Z. L. Samson, M. I. Stockman, and N. I. Zheludev, "Ultrafast active plasmonics," *Nature Photon.*, vol. 3, no. 1, pp. 55–58, 2009.

[2] N. Strohfeldt *et al.*, "Yttrium hydride nanoantennas for active plasmonics," *Nano Lett.*, vol. 14, no. 3, pp. 1140–1147, 2014.

[3] A. E. Cetin, A. A. Yanik, A. Mertir, S. Erramilli, O. E. Mustecaplioglu, and H. Altug, "Field-effect active plasmonics for ultracompact electro-optic switching," *Appl. Phys. Lett.*, vol. 101, no. 12, 2012, Art. no. 121113.

[4] Z. Wang *et al.*, "Controlling random lasing with three-dimensional plasmonic nanorod metamaterials," *Nano Lett.*, vol. 16, no. 4, pp. 2471–2477, 2016.

[5] J. Homola, S. S. Yee, and G. Gauglitz, "Surface plasmon resonance sensors: Review," *Sens. Actuators B, Chem.*, vol. 54, no. 1, pp. 3–15, 1999.

[6] M. Piliarik and J. Homola, "Surface plasmon resonance (SPR) sensors: Approaching their limits?" *Opt. Express*, vol. 17, no. 19, pp. 16505–16517, 2009.

[7] K. A. Willets and R. P. Van Duyne, "Localized surface plasmon resonance spectroscopy and sensing," *Annu. Rev. Phys. Chem.*, vol. 58, pp. 267–297, 2007.

[8] D. Ignatyeva *et al.*, "High-Q surface modes in photonic crystal/iron garnet film heterostructures for sensor applications," *JETP Lett.*, vol. 104, no. 10, pp. 679–684, 2016.

[9] A. Kar, N. Goswami, and A. Saha, "Long-range surface-plasmon-enhanced all-optical switching and beam steering through nonlinear Kerr effect," *Appl. Phys. B*, vol. 123, no. 1, 2017, Art. no. 1.

[10] J. Chen, Z. Li, S. Yue, and Q. Gong, "Highly efficient all-optical control of surface-plasmon-polariton generation based on a compact asymmetric single slit," *Nano Lett.*, vol. 11, no. 7, pp. 2933–2937, 2011.

[11] H. Lu, X. Liu, L. Wang, Y. Gong, and D. Mao, "Ultrafast all-optical switching in nanoplasmonic waveguide with Kerr nonlinear resonator," *Opt. Express*, vol. 19, no. 4, pp. 2910–2915, 2011.

[12] L. E. Kreilkamp *et al.*, "Terahertz dynamics of lattice vibrations in Au/CdTe plasmonic crystals: Photoinduced segregation of Te and enhancement of optical response," *Phys. Rev. B*, vol. 93, no. 12, 2016, Art. no. 125404.

[13] D. O. Ignatyeva and A. P. Sukhorukov, "Plasmon beams interaction at interface between metal and dielectric with saturable Kerr nonlinearity," *Appl. Phys. A*, vol. 109, no. 4, pp. 813–818, 2012.

[14] N. E. Khokhlov, D. O. Ignatyeva, and V. I. Belotelov, "Plasmonic pulse shaping and velocity control via photoexcitation of electrons in a gold film," *Opt. Express*, vol. 22, no. 23, pp. 28019–28026, 2014.

[15] V. V. Temnov *et al.*, "Active magnetoplasmonics in hybrid metal–ferromagnet structures," *Nature Photon.*, vol. 4, no. 2, pp. 107–111, 2010.

[16] D. Bossini, V. Belotelov, A. Zvezdin, A. Kalish, and A. Kimel, "Magnetoplasmonics and femtosecond optomagnetism at the nanoscale," *ACS Photon.*, vol. 3, no. 8, pp. 1385–1400, 2016.

[17] M. Shcherbakov, P. Vabishchevich, A. Y. Frolov, T. Dolgova, and A. Fedyanin, "Femtosecond intrapulse evolution of the magneto-optic Kerr effect in magnetoplasmonic crystals," *Phys. Rev. B*, vol. 90, no. 20, 2014, Art. no. 201405.

[18] A. Kalish, D. Ignatyeva, M. Bayer, V. Belotelov, L. Kreilkamp, and A. Sukhorukov, "Transformation of mode polarization in gyrotropic plasmonic waveguides," *Laser Phys.*, vol. 24, no. 9, 2014, Art. no. 094006.

[19] D. O. Ignatyeva, A. N. Kalish, G. Y. Levkina, and A. P. Sukhorukov, "Surface plasmon polaritons at gyrotropic interfaces," *Phys. Rev. A*, vol. 85, 2012, Art. no. 043804.

[20] G. Mi and V. Van, "Characteristics of surface plasmon polaritons at a chiral–metal interface," *Opt. Lett.*, vol. 39, no. 7, pp. 2028–2031, 2014.

[21] D. Ignatyeva, A. Kalish, V. Belotelov, and A. Zvezdin, "Polarization properties of surface plasmon polaritons at the boundary of topological insulators with the axion effect," *Phys. Wave Phenom.*, vol. 25, no. 2, pp. 119–123, 2017.

[22] R. H. Tarkhanyan and D. G. Niarchos, "Nonradiative surface electromagnetic waves at the interface of uniaxially bianisotropic enantiomeric media," *Phys. Status Solidi B*, vol. 248, no. 6, pp. 1499–1504, 2011.

[23] V. M. Galynsky, A. Furs, and L. Barkovsky, "Integral formalism for surface electromagnetic waves in bianisotropic media," *J. Phys. A, Math. Gen.*, vol. 37, no. 18, pp. 5083–5096, 2004.

[24] A. M. Shuvaev, S. Engelbrecht, M. Wunderlich, A. Schneider, and A. Pimenov, "Strong dynamic magnetoelectric coupling in metamaterial," *Eur. Phys. J. B*, vol. 79, no. 2, pp. 163–167, 2011.

[25] A. Popkov, M. Davydova, K. Zvezdin, S. Solov'yov, and A. Zvezdin, "Origin of the giant linear magnetoelectric effect in perovskitelike multiferroic $BiFeO_3$," *Phys. Rev. B*, vol. 93, no. 9, 2016, Art. no. 094435.

[26] M. Bichurin and D. Viehland, *Magnetoelectricity in Composites*. Boca Raton, FL, USA: CRC Press, 2011.

[27] G. Sreenivasulu, V. Petrov, L. Fetisov, Y. Fetisov, and G. Srinivasan, "Magnetoelectric interactions in layered composites of piezoelectric quartz and magnetostrictive alloys," *Phys. Rev. B*, vol. 86, no. 21, 2012, Art. no. 214405.

[28] M. Lorenz *et al.*, "Correlation of magnetoelectric coupling in multiferroic $batio_3$-$bifeo_3$ superlattices with oxygen vacancies and antiphase octahedral rotations," *Appl. Phys. Lett.*, vol. 106, no. 1, 2015, Art. no. 012905.

[29] W. Eerenstein, N. Mathur, and J. F. Scott, "Multiferroic and magnetoelectric materials," *Nature*, vol. 442, no. 7104, pp. 759–765, 2006.

[30] R. Pisarev, "Crystal optics of magnetoelectrics," *Ferroelectrics*, vol. 162, no. 1, pp. 191–209, 1994.

[31] M. Fiebig, "Revival of the magnetoelectric effect," *J. Phys. D, Appl. Phys.*, vol. 38, no. 8, pp. R123–R152, 2005.

[32] T. Ashida, M. Oida, N. Shimomura, T. Nozaki, T. Shibata, and M. Sahashi, "Observation of magnetoelectric effect in Cr_2O_3/Pt/Co thin film system," *Appl. Phys. Lett.*, vol. 104, no. 15, 2014, Art. no. 152409.

[33] F. Wilczek, "Two applications of axion electrodynamics," *Phys. Rev. Lett.*, vol. 58, no. 18, pp. 1799–1802, 1987.

[34] R. Li, J. Wang, X.-L. Qi, and S.-C. Zhang, "Dynamical axion field in topological magnetic insulators," *Nature Phys.*, vol. 6, no. 4, pp. 284–288, 2010.

[35] M. Z. Hasan and C. L. Kane, "Colloquium: Topological insulators," *Rev. Mod. Phys.*, vol. 82, no. 4, pp. 3045–3067, 2010.

[36] Y.-W. Huang *et al.*, "Design of plasmonic toroidal metamaterials at optical frequencies," *Opt. Express*, vol. 20, no. 2, pp. 1760–1768, 2012.

[37] N. Gusev, V. Belotelov, and A. Zvezdin, "Surface plasmons in nanowires with toroidal magnetic structure," *Opt. Lett.*, vol. 39, no. 14, pp. 4108–4111, 2014.

[38] F. W. Hehl, Y. N. Obukhov, J.-P. Rivera, and H. Schmid, "Relativistic nature of a magnetoelectric modulus of Cr_2O_3 crystals: A four-dimensional pseudoscalar and its measurement," *Phys. Rev. A*, vol. 77, no. 2, 2008, Art. no. 022106.

[39] Y. F. Popov, A. Kadomtseva, D. Belov, G. Vorobev, and A. Zvezdin, "Magnetic-field-induced toroidal moment in the magnetoelectric Cr_2O_3," *J. Exp. Theor. Phys. Lett.*, vol. 69, no. 4, pp. 330–335, 1999.

[40] H. Wiegelmann, A. Jansen, P. Wyder, J.-P. Rivera, and H. Schmid, "Magnetoelectric effect of Cr_2O_3 in strong static magnetic fields," *Ferroelectrics*, vol. 162, no. 1, pp. 141–146, 1994.

[41] B. Krichevtsov, V. Pavlov, R. Pisarev, and V. Gridnev, "Spontaneous nonreciprocal reflection of light from antiferromagnetic Cr_2O_3," *J. Phys., Condens. Matter*, vol. 5, no. 44, pp. 8233–8244, 1993.

[42] S. Foner and M. Hanabusa, "Magnetoelectric effects in Cr_2O_3 and $(Cr_2O_3)_{0.8}\cdot(Al_2O_3)_{0.2}$," *J. Appl. Phys.*, vol. 34, no. 4, pp. 1246–1247, 1963.

[43] M. Fiebig, D. Fröhlich, and H.-J. Thiele, "Determination of spin direction in the spin-flop phase of Cr_2O_3," *Phys. Rev. B*, vol. 54, no. 18, pp. R12681–R12684, 1996.

[44] J. Polo, T. Mackay, and A. Lakhtakia, *Electromagnetic Surface Waves: A Modern Perspective*. Waltham, MA, USA: Newnes, 2013.

[45] V. Dubovik and V. Tugushev, "Toroid moments in electrodynamics and solid-state physics," *Phys. Rep.*, vol. 187, no. 4, pp. 145–202, 1990.

[46] W.-K. Tse and A. MacDonald, "Giant magneto-optical Kerr effect and universal faraday effect in thin-film topological insulators," *Phys. Rev. Lett.*, vol. 105, no. 5, 2010, Art. no. 057401.

[47] M.-C. Chang and M.-F. Yang, "Optical signature of topological insulators," *Phys. Rev. B*, vol. 80, no. 11, 2009, Art. no. 113304.

[48] F. Liu, J. Xu, and Y. Yang, "Polarization conversion of reflected electromagnetic wave from topological insulator," *J. Opt. Soc. Amer. B*, vol. 31, no. 4, pp. 735–741, 2014.

[49] A. N. Kalish, V. I. Belotelov, and A. K. Zvezdin, "Optical properties of toroidal media," *Proc. SPIE*, vol. 6728, 2007, Art. no. 67 283D.

[50] M. Liscidini and J. Sipe, "Quasiguided surface plasmon excitations in anisotropic materials," *Phys. Rev. B*, vol. 81, no. 11, 2010, Art. no. 115335.

[51] V. Belotelov *et al.*, "Enhanced magneto-optical effects in magnetoplasmonic crystals," *Nature Nanotechnol.*, vol. 6, no. 6, pp. 370–376, 2011.

Authors' biographies not available at the time of publication.